Received: 27 May 2021 | Revised: 15 September 2021 | Accepted: 29 September 2021

DOI: 10.1002/pip.3493

RESEARCH ARTICLE

PROGRESS IN PHOTOVOLTAICS WILEY

# A route towards high-efficiency silicon heterojunction solar cells

Weiyuan Duan | Andreas Lambertz | Karsten Bittkau | Depeng Qiu | Kaifu Qiu | Uwe Rau | Kaining Ding

IEK-5 Photovoltaik, Forschungszentrum Jülich GmbH, Jülich, Germany

**Correspondence**
Weiyuan Duan, IEK-5 Photovoltaik, Forschungszentrum Jülich GmbH, 52428 Jülich, Germany.
Email: w.duan@fz-juelich.de

**Funding information**
German Federal Ministry of Economic Affairs and Energy, Grant/Award Numbers: 0324351, 0324198D, 0324275E

## Abstract

In this work, we propose a route to achieve a certified efficiency of up to 24.51% for silicon heterojunction (SHJ) solar cell on a full-size n-type M2 monocrystalline-silicon Cz wafer (total area, 244.53 $cm^2$) by mainly improving the design of the hydrogenated intrinsic amorphous silicon (a-Si:H) on the rear side of the solar cell and the back reflector. A dense second intrinsic a-Si:H layer with an optimized thickness can improve the vertical carrier transport, resulting in an improved fill factor (*FF*). In order to reduce the plasmonic absorption at the back reflector, a low-refractive-index magnesium fluoride ($MgF_2$) is deposited before the Ag layer; this leads to an improved gain of short circuit current density ($J_{sc}$). In total, together with $MgF_2$ double antireflection coating and other fine optimizations during cell fabrication process, ~1% absolute efficiency enhancement is finally obtained. A detailed loss analysis based on Quokka3 simulation is presented to confirm the design principles, which also gives an outlook of how to improve the efficiency further.

**KEYWORDS**
amorphous silicon, back reflector, design, loss analysis, silicon heterojunction solar cells

## 1 | INTRODUCTION

As one of the technologies with passivating contacts, silicon heterojunction (SHJ) solar cell technology is considered to expand its share in the PV industry in the coming years due to the high-power conversion efficiency, lean fabrication process, and low temperature coefficient.[1,2] High efficiency is the biggest advantage of SHJ solar cells, which increases their competitiveness for mass production. In recently years, milestones with certified SHJ solar cell efficiency of more than 24.5% have been reported by several organizations. For examples, Panasonic announced 24.7% conversion efficiency based on 98-μm thin wafers as early in 2013.[3] Then in 2015, Kaneka reported the record efficiency of 25.1% with aperture area of 151.9 $cm^2$ by electrical copper plating.[4] In 2019 and 2020, Hanergy set two times world records in a row, reported full M2 area (244.5 $cm^2$) efficiency of 24.85% and 25.1%, respectively.[5,6] This result once again brings to light the potential for heterojunction solar cell efficiency improvement. In the beginning of this year, GS-Solar has announced that the conversion efficiency of its mass produced SHJ solar cells has reached 25.2%, which has been certified by TÜV Nord.[7] The very high fill factor (*FF*) of 85.82% makes it as the record for mass-produced SHJ solar cells on the market. Recently, SunDrive has rocked the status quo, developed a silver-free SHJ cell and at the same time elevating the world efficiency record for a commercial-size to 25.54%.[8] These reported high efficiencies motivate us to go deeper into the knowledge behind the development.

SHJ solar cells have an excellent open-circuit voltage ($V_{oc}$) of up to 750 mV[3] due to the superior silicon interface passivation provided by thin hydrogenated amorphous silicon (a-Si:H) layers, which has contributed significantly to the success of this architecture. However, the SHJ solar cells show a lower short-circuit current density ($J_{sc}$) compared with the other two sides contacted crystalline silicon cells which is a result of the parasitic absorption due to the front a-Si:H layers and transparent conductive oxide (TCO) layers on both sides.[9,10] To improve $J_{sc}$, previous work mostly focused on developing more transparent window layers, such as replacing doped a-Si:H by hydrogenated nano-crystalline silicon oxide (nc-$SiO_x$:H).[11–13] These approaches encountered challenges of how to achieve trade-off between optical and electrical properties[14,15] and industrial application issues like the process time.[16] Besides, even though high *FF* can be achieved among aforementioned champion efficiencies, there is still a gap to the reported theoretical *FF* of 88%–89%,[17] which needs to be engineered further.

In this work, starting from a certified cell efficiency of 23.55% with $V_{oc}$ of 741.2 mV, $J_{sc}$ of 38.94 mA/cm$^2$, and *FF* of 81.85% measured in the certification lab CalTeC at Institute for Solar Energy Research in Hamelin (ISFH), a route towards higher efficiency SHJ solar cell is proposed through a combination of device simulation and experimental work. Comparing the certified result with the other high-efficiency SHJ solar cells or theoretical values, it can be found that the difference in $V_{oc}$ is minimal; however, the gap in $J_{sc}$ and *FF* shows potential for significant improvement in efficiency. Performing a detailed power loss analysis (will be shown in Figure 7) of the cell revealed that reflection, light trapping and parasitic absorption dominate the current loss, and rear TCO/silicon vertical transport loss dominate the loss in *FF*. The method of looking for transparent thin films to reduce the parasitic absorption is always contradicting with reducing series resistance ($R_s$) loss by implementing high conductive thin film layers. Thus, in this work, to avoid complicated consideration for the trade-off of film optoelectrical performance, an alternative route towards high-efficiency (>24.5%) rear emitter SHJ solar cells is rolled out. We have focused on the impact of rear side double intrinsic a-Si:H layers (basically no effect on cell optics) and an optimized metal back reflector on the solar cell performance. An inclusive analysis during these developments is shown, together with a newly certified champion efficiency of 24.51% on a M2-size n-type crystalline wafer (total area, 244.53 cm$^2$). Last but not least, the prospect to even high-efficiency SHJ solar cell is also discussed with insights into the loss analysis by simulation.

## 2 | EXPERIMENTAL AND SIMULATION METHODS

During the study, all SHJ solar cells were fabricated using M2-size n-type Czochralski (CZ) crystalline silicon as-cut wafers from LONGi company, with resistivity of 1–5 Ωcm and a thickness of 180 μm. The wafers were firstly chemically etched to remove saw damage and then textured in alkaline solution to obtain random pyramids on both sides. After ozone cleaning finalized with a 1% diluted hydrofluoric acid solution, the wafers were transported into an AK 1000 plasma enhanced chemical vapor deposition (PECVD) tool from Meyer Burger for intrinsic and doped a-Si:H fabrication. Here, intrinsic a-Si:H bi-layers were used in the structure; the silane ($SiH_4$)/hydrogen ($H_2$) flow ratio and thickness were varied for the second layer of intrinsic a-Si:H bi-layers deposition, which will be discussed in details in the following content. Afterwards, 70-nm indium tin oxide (ITO) layers were sputtered from an 3% Sn-doped $In_2O_3$ target onto both sides of the wafers with a direct current mode. During the sputtering process, the oxygen has a partial pressure of 0.016 Pa, calculated from a working pressure of 0.3 Pa and a fixed total Ar and oxygen flow rate of 95 sccm. The ITO layers used in the device has a mobility of 28 cm$^2$/Vs and carrier density of $1.5 \times 10^{20}$ cm$^{-3}$. Then silver grids with a busbar-less design were screen printed on both sides of the ITO layers and subsequently cured at 170°C for 40 min in air atmosphere. The cells have a finger width of 40 μm and finger pitch of 1.6 mm for the front side, and a finger width of 80 μm and finger pitch of 0.6 mm for the rear side. A very transparent $MgF_2$ layer with a thickness of 100 nm was sputtered on the top of the front ITO to act as a second antireflection coating layer. Part of the cells got a full area 200 nm evaporated Ag layer on the rear side, which acts together with ITO as a back reflector. For some of the other cells, a 70-nm $MgF_2$ layer was deposited before the Ag layer evaporation. The metallization curing process for cells with $MgF_2$ was taken place after $MgF_2$ deposition instead of directly after screen printing, in order to fire the grids through the insulated $MgF_2$ layer. Finally, the cells were exposed in 1 sun light intensity for 20 h to complete the light soaking process. The structure of the final certified SHJ solar cell has a rear-emitter design as shown in Figure 1A.

For material characterization, intrinsic a-Si:H films with thickness of 15 nm were deposited on polished float-zone crystalline silicon wafers. The thickness of the films was extracted from ellipsometer (J. A. Woollam M-2000) measurement. Structural characterization of the local bonding environments was performed by Fourier Transform Infrared Spectroscopy (FTIR) in a Nicolet 5700 system with wavenumber scanned from 400 cm$^{-1}$ to 4000 cm$^{-1}$. To evaluate the solar cells performance, current–voltage (*J-V*) characteristics were measured under standard test conditions (AM1.5, 25°C and 100 mW/cm$^2$) by the integrated solar cell characterization system called LOANA from pv-tools with a Wavelabs Sinus 220 light source. The series resistance was extracted from a set of *J-V* curves attained at different illumination intensities. Furthermore, the external quantum efficiency (*EQE*) and reflectance (*Ref*) were measured on a 20 × 20 mm$^2$ area on the cells with grids inside. To determine the contact resistance of the cells, the transfer-length-method (TLM)[18] contact pad arrays were used, which were made by sputtering ITO and screen-printing Ag through a shadow mask. The TLM pattern is illustrated in Figure 1B. When voltage is applied on the contacts, the current flows across the thin films and transport through the wafer between the contacts. The measured contact resistance will be the total vertical transport resistance.

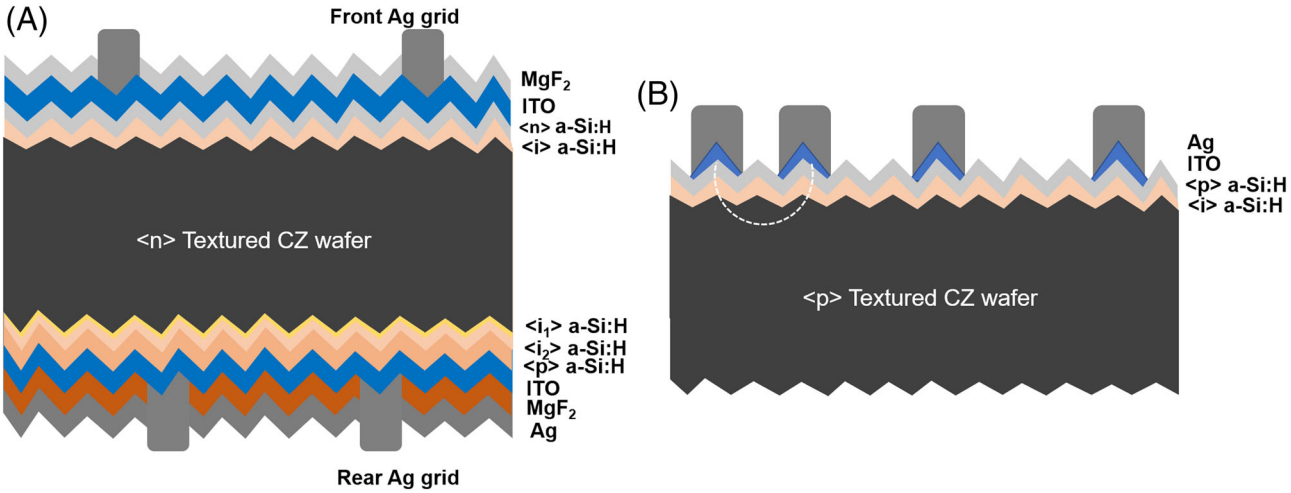


**FIGURE 1** (A) Cross-sectional sketch of the certified SHJ solar cell and (B) TLM pattern structure

The power loss mechanism of the SHJ solar cells was identified and simulated by the commercial device simulator Quokka3,[19,20] which is a fast tool for simulating 2D/3D carrier transport in silicon solar cell devices. It is enabled by the skin concept where the skins are numerically treated as a parameterized boundary conditions when solving carrier transport in the bulk. The lumped skins are characterized mainly by their sheet resistance obtained from four-point probe measurement and recombination properties determined from quasi steady state photoconductivity (QSSPC) measurement.

## 3 | RESULTS AND DISCUSSION

### 3.1 | Intrinsic a-Si:H bi-layers

The intrinsic a-Si:H layer plays multiple roles in SHJ solar cells not only as a surface passivation layer but also as a carrier transport channel to the electrode. In general, a high-quality intrinsic a-Si:H material with denser microstructure is beneficial for cell performance.[21,22] However, the direct growth of this type of material on the crystalline silicon surface can easily lead to epitaxial growth at the interface, which would be detrimental for surface passivation.[23] Intrinsic a-Si:H with a porous interfacial layer can improve the surface passivation by suppressing epitaxial crystallization, however it causes an increase in series resistance.[24] To balance passivation and charge carrier transport, intrinsic a-Si:H bi-layers with a porous first layer and a dense second layer are a viable route. Beside the microstructure of intrinsic a-Si:H, its thickness also plays an important role in solar cell performance due to the low conductivity. The optimum thickness of intrinsic a-Si:H would result in sufficient passivation without excessive series resistance loss. Based on these design principles, intrinsic a-Si:H bi-layers were used in our SHJ solar cell structure, and the microstructure and thickness of the second intrinsic a-Si:H ($i_2$), used on the rear side of the cells, were specially optimized here to reduce the vertical charge carrier transport loss.

To investigate the microstructure of the intrinsic a-Si:H thin films, the absorption coefficient spectra versus wavelength of a-Si:H films obtained by FTIR spectroscopy is shown in Figure 2. Among them, Figure 2A,B shows the results of the first intrinsic a-Si:H ($i_1$) layer and the originally used $i_2$ layer, respectively. Then the $SiH_4/H_2$ flow ratio for $i_2$ layer has been decreased, resulting in a different microstructure as shown in Figure 2C,D. Curve fitting using Gaussian functions has been performed to determine the strength of the low-stretching mode (LSM) and the high-stretching mode (HSM) centered at wavenumbers of around 2000 $cm^{-1}$ and 2100 $cm^{-1}$, respectively.[25] The LSM represents the vibration of compact hydrogen (monohydrides) incorporation, while the HSM is attributed to the vibrations of hydrogen clusters (dihydrides, trihydrides) grouped together at the surfaces of nano-sized voids.[26–28] The microstructure factor R is defined as $R = I_{HSM}/(I_{LSM} + I_{HSM})$, where $I_{LSM}$ and $I_{HSM}$ are absorption peak intensities of the low- and high-stretching modes.[29] In this definition, the larger R means the higher the density of nano-sized voids in the a-Si:H films. Figure 2 shows R of 0.68 for $i_1$ layer and 0.32 for the original $i_2$ layer. The large R of $i_1$ layer reveals a porous intrinsic a-Si:H layer used on the crystalline silicon surface. Slightly decreasing the $SiH_4/H_2$ ratio to 1/6.2 for $i_2$ layer significantly decreased the R from 0.32 to 0.19. This is mainly due to the etching effect from more hydrogen plasma, which breaks up weak Si-bonded hydrogen in the formation of clusters, making the film denser. Further decreasing the $SiH_4/H_2$ ratio will again increase the void density in the film (larger R), result a porous film. This may be caused by the incorporation of excessive hydrogen due to high hydrogen plasma treatment during the deposition.[30]

The effect of $i_2$ layer with different $SiH_4/H_2$ flow ratio and thickness on SHJ solar cell performances were verified by six bifacial cells without a second antireflection coating layer for each group, and the *J-V* parameters in (a) $V_{oc}$, (b) $J_{sc}$, (c) *FF* and pseudo *FF* (*pFF*), (d) the conversion efficiency ($\eta$), and (e) $R_s$ were summarized as shown in Figure 3. First, the original thickness of $i_2$ layer ($d_{i2}$) was fixed at 7 nm. The $V_{oc}$ of the cells remained constant within the statistical

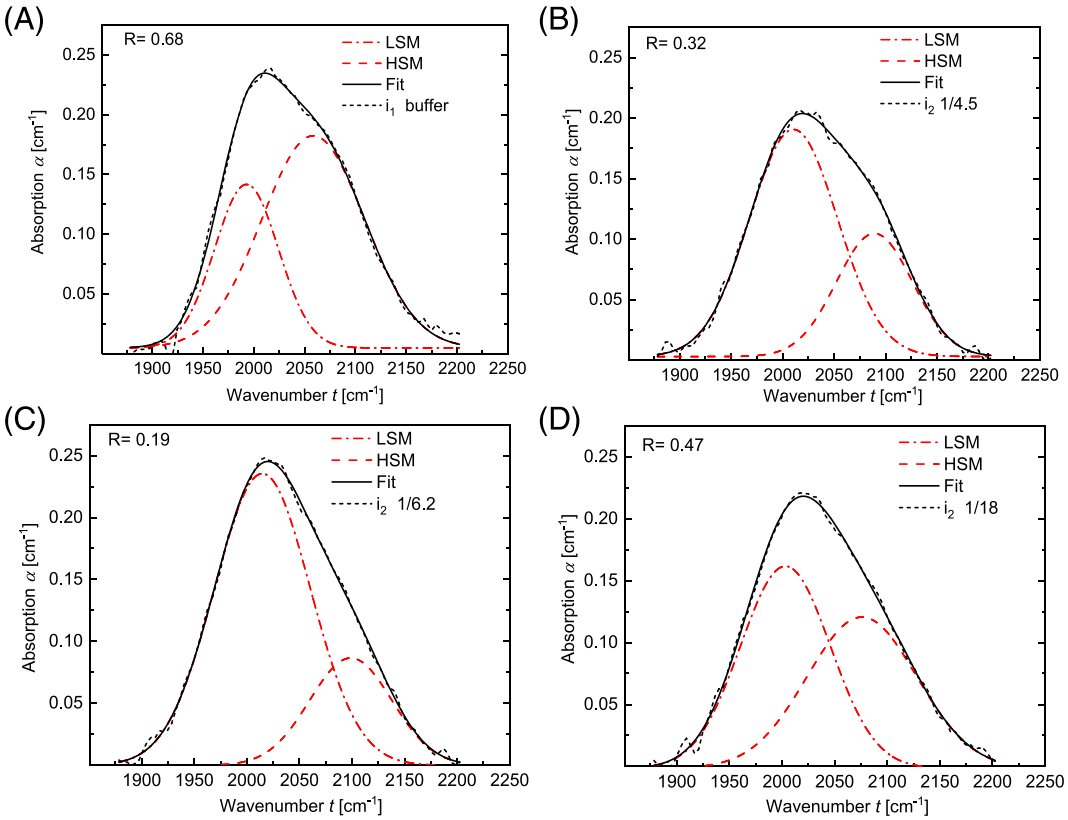


**FIGURE 2** Absorption coefficient spectra obtained by FTIR for (A) the first intrinsic a-Si:H ($i_1$) layer and (B, C, D) the second intrinsic a-Si:H ($i_2$) layers with a variation of $SiH_4/H_2$ flow ratio, fitted with two Gaussian-distributed absorption peaks centered at wavenumbers of 2000 $cm^{-1}$ for low-stretching mode (LSM) and 2100 $cm^{-1}$ for high-stretching mode (HSM). R is the microstructure factor which is defined as the peak intensity of HSM divided by the sum of peak intensity of HSM and LSM

fluctuation when varying the $SiH_4/H_2$ flow ratio, which indicated a similar passivation despite of the microstructure factor variation. Similar to $V_{oc}$, the $J_{sc}$ also showed almost no difference by changing the R of $i_2$ layer on the rear side of the cells. More clearly, significantly increased *FF* was obtained when decreasing the $SiH_4/H_2$ ratio from 1:4.5 to 1:6.2 with R reduced from 0.32 to 0.19. The improvement of *FF* is mainly due to the reduced $R_s$ as shown in Figure 3E while *pFF* is kept constant, which was related to the enhanced charge carrier transport due to denser $i_2$ layer with lower defect density (smaller R) on the rear side. This was also confirmed by reduced whole rear vertical contact resistance from 350 to 180 $m\Omega.cm^2$ measured by TLM as shown in Figure 1B. When further decreasing of $SiH_4/H_2$ ratio, the excessive hydrogen makes the film more porous, which is not beneficial for carrier transport. However, excessive hydrogen could also bring severe etch effect, which can slightly decrease the thickness of intrinsic a-Si:H layer with poor conductivity.[31] That is probably the reason for the continuous drop of $R_s$. However, this also caused a compromise of passivation which can be seen from the slightly drop of *pFF*. As a consequence, the *FF* did not really show an advantage when the $SiH_4/H_2$ ratio of $i_2$ layer decreased to 1:18. Based on this, the thickness of $i_2$ layer was further optimized for fine tuning with $SiH_4/H_2$ ratio of 1:6.2. By reducing the thickness from 7 nm to 5.6 nm, slightly higher averaged *FF* value with less deviation was obtained, and passivation was maintained as can be seen from the *pFF*. The decrease of $R_s$ loss is responsible for the improvement of *FF*. However, the passivation or effective space charge area cannot be maintained by further decreasing the $i_2$ layer thickness to 4.6 nm, resulting in a deterioration in $V_{oc}$, $J_{sc}$, and *pFF*. Even though at this parameter $R_s$ shows the lowest value, the *FF* is mainly affected by the decreased *pFF*. Finally, the average conversion efficiency of SHJ solar cells has increased from 23.35% to 23.70% by optimizing the $i_2$ layer, where a trade-off between passivation and carrier transport has been achieved.

## 3.2 | Back reflector

Crystalline silicon solar cells have poor conversion for wavelengths near the active-layer bandgap, motivating light management studies in the infrared range.[32] Especially for SHJ solar cells which require TCO layers at the front and rear to transport charge carriers laterally, free charge carriers in these layers absorb infrared light which can hardly contribute to the current generation of the solar cell. The infrared light management for bifacial SHJ solar cells includes reducing the parasitic absorption and minimizing the potion of escaped light as well. There is always a limit in developing more transparent thin film

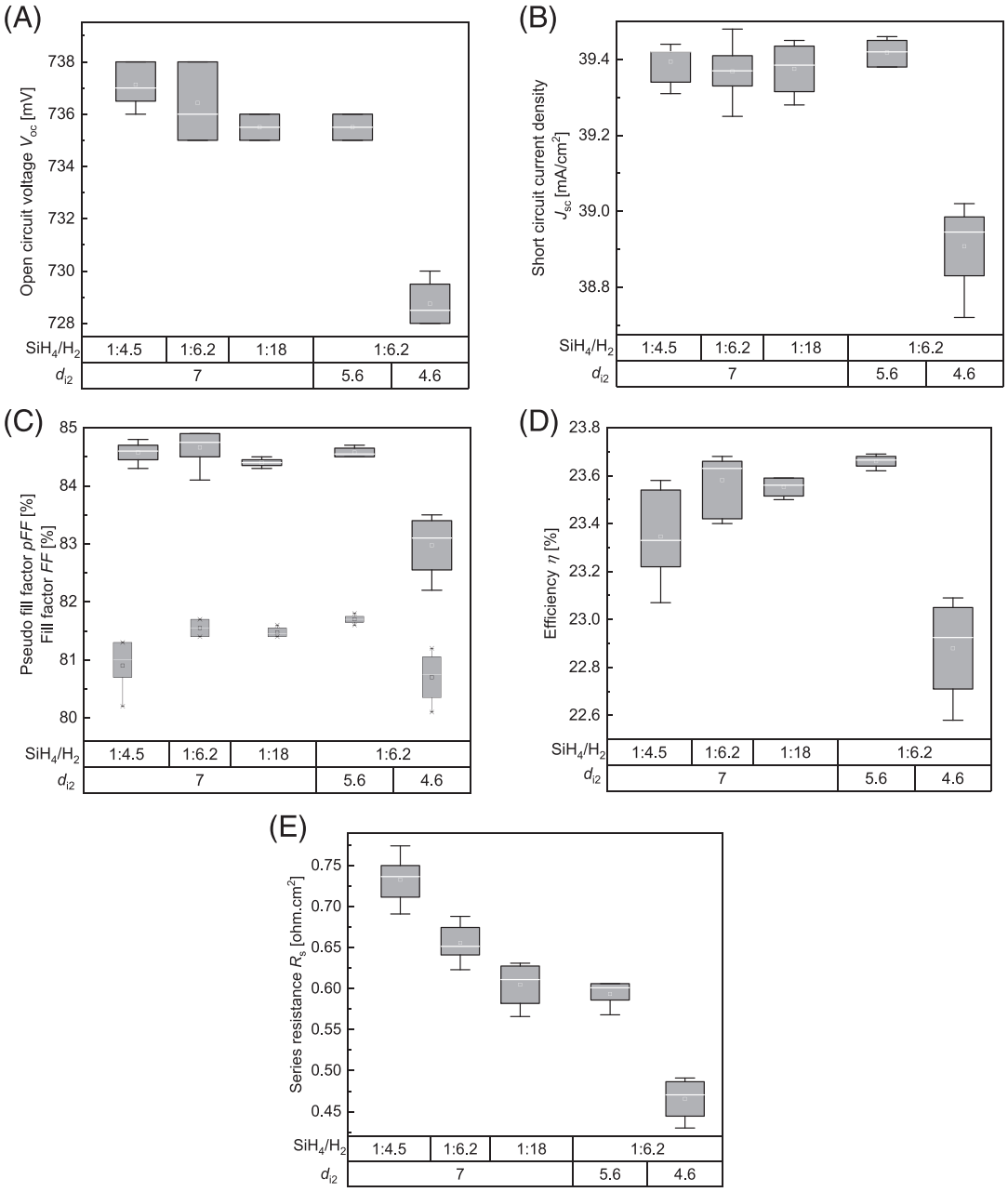


**FIGURE 3** J-V parameters: (A) $J_{sc}$, (B) $V_{oc}$, (C) *FF*/*pFF*, (D) η, and (E) $R_s$ of SHJ solar cells fabricated as a function of $SiH_4/H_2$ flow ratio and thickness of the $i_2$ layer ($d_{i2}$)

layers, since a tradeoff between optical and electrical performance has to be considered, as more transparent layers often result in lower conductivities.[33] Thus, to increase the optical pathlength by reducing the escaped light in the infrared region seems to be a more independent way to increase current generation. In SHJ solar cells, full area Ag after TCO layer typically acts as a back reflector and contact. However, plasmonic absorption at the rough TCO/metal interface induced by light scattering of evanescent waves has been reported,[34,35] making the effect of back reflection much less effective. In cells like passivated emitter with rear locally diffused (PERL) cells, the silicon nitride, silicon dioxide or aluminum oxide rear passivation layer simultaneously enhances reflectance since these dielectric layers can limit the cone of light that is transmitted to the lossy metal electrode.[36–38] From a purely optical perspective, the best rear dielectric layer for solar cells with micrometer-sized or larger rear textures should have the lowest possible refractive index.[39] Campbell et al hypothesized excellent internal reflectance by inserting a layer of low-refractive-index $MgF_2$ between the rear passivation layer and aluminum rear electrode in PERL-like cells.[40] Here, 70-nm $MgF_2$ was introduced before 200-nm Ag back reflector evaporated on the bifacial cells. During cell fabrication, the curing process for rear printed fingers was done after $MgF_2$ evaporation in order to fire the fingers through

the insulated material and make a reliable contact to following layer. For comparison, SHJ solar cells with only 200-nm Ag layer were also prepared, the relative change of cell performance to standard bifacial reference cell is shown in Figure 4. It is necessary to mention that the cells here already had $MgF_2$ double antireflection coating on the front. As revealed by the results, there was no compromise for *FF* when introducing either of the two back reflectors, which demonstrates that no extra resistive loss was induced by inserting an insulated layer before the full area Ag. The slightly higher $V_{oc}$ for cells with rear $MgF_2$ might be related to the extra annealing during the film evaporation process. The maximum absolute increase of $J_{sc}$ was 0.45 mA/cm$^2$ for cells with only Ag back reflector. A higher gain of 0.63 mA/cm$^2$ was achieved after introducing the thin $MgF_2$ layer before Ag. Overall, the efficiency improvement mainly came from the $J_{sc}$ gain. Cells with $MgF_2$/Ag back reflector could increase the efficiency by relative 2%, which is a very attractive method of further gaining cell efficiency for monofacial application cases.

Figure 5 shows *EQE* and 1-*Ref* spectra before and after Ag and $MgF_2$/Ag preparation, respectively, to figure out how different back reflectors affect light management. By comparing the solid lines before preparation of back reflectors and the dashed lines with reflectors, the main differences came from the infrared region, where *EQE* and the escaped reflectance all increased. After introducing Ag or $MgF_2$/Ag layers, ITO together with the layers acted as back reflectors. The transmittance loss was transferred to the increased internal reflection and parasitic absorption (including parasitic absorption in layers and plasmonic absorption) in the back reflectors. Even though higher internal reflectance would cause higher escaped reflectance, still part of the photons had been successfully absorbed by silicon bulk and transferred to charge carrier generation as *EQE* all improved, which was the source of $J_{sc}$ enhancement. After introducing a 70-nm $MgF_2$ between the rear ITO and Ag layer, the escaped reflectance increased further as shown by comparing the red and black dashed lines. This was mainly due to the increased internal reflectance by reducing the plasmonic absorption on the Ag surface with this low-refractive-index dielectric material. Normally, the gap between the *EQE* and 1-*Ref* curves accounts for the parasitic loss as well as transmission loss. The transmission loss decreased to zero after adding back reflectors, so the gap here only represents the parasitic loss (total parasitic absorption) in the back reflectors.[41] This also confirmed a reduced plasmonic absorption with adding this 70 nm $MgF_2$ before Ag evaporation. As shown from the black and red dashed lines, the total parasitic absorption decreased after inserting $MgF_2$ layer with both superior *EQE* and escaped reflectance, which means part of the reduced plasmonic absorption had been transferred to charge carrier generation which contributed to the further increase in $J_{sc}$. By matching the thickness of ITO and $MgF_2$ may enhance the $J_{sc}$ gain even further. It should be noted that the electrical properties such as the lateral transport of ITO layer and how to fire electrodes through $MgF_2$ layer need to be considered during this optimization, which requires more experiments in the future.

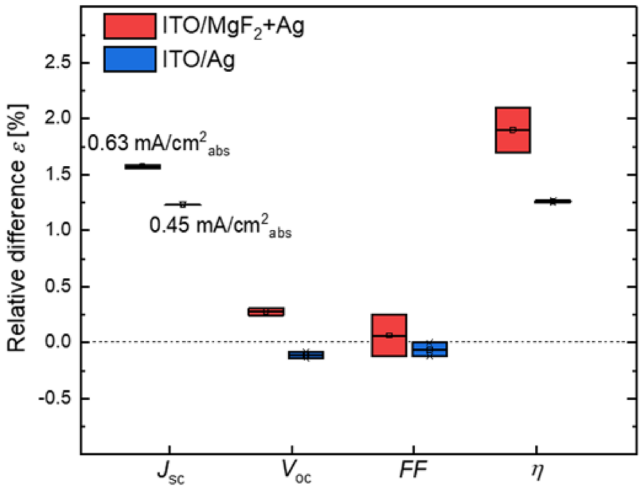


**FIGURE 4** Relative difference of solar cell parameters after introducing ITO/Ag (blue symbols) or ITO/$MgF_2$ + Ag (red symbols) back reflectors compared with cells with no back reflector

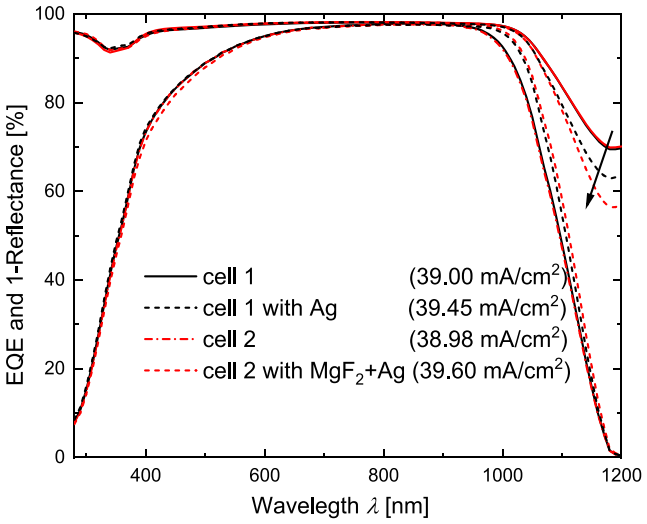


**FIGURE 5** External quantum efficiency and 1-Reflectance of SHJ solar cells before (solid) and after (dashed) different back reflector preparation. The black lines represent cells with and without Ag reflector, and the red lines represent cells with and without $MgF_2$ + Ag reflector

## 3.3 | Power loss analysis

Based on the aforementioned optimization, by combining with other fine-tuning steps, such as environment control, proper wafer handling and the 1 sun light curing which slightly reduces the series resistance loss as also presented by the others' research,[42] eventually we have brought the certified SHJ solar cell efficiency from 23.55% (with $I_{sc}$ of 9519 mA, $V_{oc}$ of 741.2 mV and *FF* of 81.58%) to 24.51% on total area of 244.5 cm$^2$ measured at ISFH. This cell has $I_{sc}$ of 9663 mA, $V_{oc}$ of 741.8 mV, and *FF* of 83.61% as shown in Figure 6.

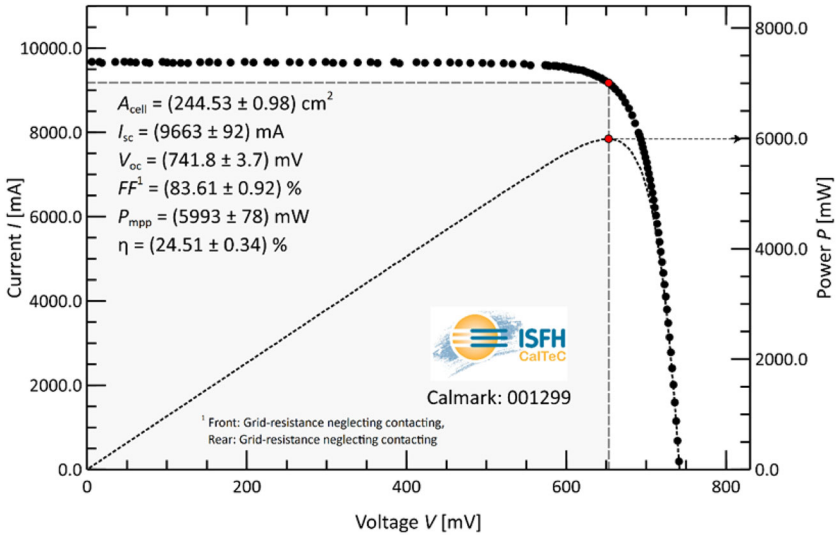


**FIGURE 6** I-V characteristics of the 24.51% efficiency SHJ solar cell certified by ISFH CalTeC

A detailed loss analysis for these two certified cells has been conducted by using Quokka3 simulation tool. The main input parameters for the simulation are listed in Table 1. The measured *EQE* and layer properties of the thin films were considered to properly describe front layer transmission losses and light-trapping parameters in Quokka3. Figure 7A,B shows the current and free energy losses for the old and newly certified full-size cells with busbar less design. Figure 7A reveals that the main optical loss aroused from external reflection and parasitic absorption for the 23.55% cell, which has been significantly reduced by applying the $MgF_2$ double antireflection coating layer on the newly certified 24.51% cell. The transmission loss at the back reflector or light that is reflected at the rear side and escaping at the front contributed to the "light trapping loss". In the cell with $MgF_2$ double antireflection coating and optimized back reflector, this loss was very similar to the original bifacial cell as shown in Figure 7A. The reason was that there were two effects, reduction of transmission loss and reduction of reflection loss at the front coming together for the newly certified cell. The reduction of transmission loss would reduce the light trapping loss; however, the reduction of reflection loss would increase the amount of light which couples into the cell, therefore also scaled up the generated current. Even though the "light trapping loss" had a similar absolute value for these two cells, the ratio between the loss and whole generated current was actually decreased for the newly certified cell due to reduced optical loss by putting the back reflector. The main electrical loss relating to the rear TCO/a-Si:H contact resistance was dramatically reduced for the newly certified cell as shown in Figure 7B, owing to the optimized $i_2$ layer on the rear side, which was consistent with the aforementioned material and device results in Figure 2 and Figure 3. In addition, slightly better passivation was also found, attributed to the better handling such as avoiding obvious scratches of tweezers on the wafer edge. To further improve the solar cell efficiency, based on the optical analysis, more efforts need to be made to reduce the parasitic absorption, such as replacing the doped a-Si:H layer with a more transparent nc-$SiO_x$:H layer. From electrical point of view, except using higher quality wafer, optimization of the front TCO layer may give slightly higher chance to increase

**TABLE 1** Input parameter set for Quokka3 simulation

| | Cell efficiency of 23.55% | Cell efficiency of 24.51% |
|---|---|---|
| Bulk resistivity (Ωcm) | 1.079 | 1.067 |
| Bulk fixed lifetime (ms) | 30,000 | 30,000 |
| Optical Z0 | 25.5 | 26 |
| Optical Zinf | 1.5 | 1 |
| Optical Zp | 1.2 | 1 |
| Optical Jgen (mA/cm²) | 39.97 | 40.56 |
| Front skin Rsheet (Ω) | 160 | 130 |
| Front skin resistivity (Ω.cm²) | 0.17 | 0.15 |
| Front skin contacted Seff (cm/s) | 1 | 0.7 |
| Front skin non-contacted Seff (cm/s) | 1 | 0.7 |
| Rear skin Rsheet (Ω) | 160 | 130 |
| Rear skin resistivity (Ω.cm²) | 0.35 | 0.105 |
| Rear skin contacted Seff (cm/s) | 1 | 0.7 |
| Rear skin non-contacted Seff (cm/s) | 1 | 0.7 |
| Front contact geometry | rectangle | rectangle |
| Front contact pitch (μm) | 1600 | 1600 |
| Front contact resistivity (Ω.cm²) | 0.001 | 0.001 |
| Front contact size (μm) | 40 | 40 |
| Front contact Rsheet (Ω) | 1.00E−06 | 1.00E−06 |
| Rear contact geometry | rectangle | rectangle |
| Rear contact pitch (μm) | 600 | 600 |
| Rear contact resistivity (Ω.cm²) | 0.001 | 0.001 |
| Rear contact size (μm) | 80 | 80 |
| Rear contact Rsheet (Ω) | 1.00E−06 | 1.00E−06 |
| Optical shading fraction | 0.92 | 0.92 |

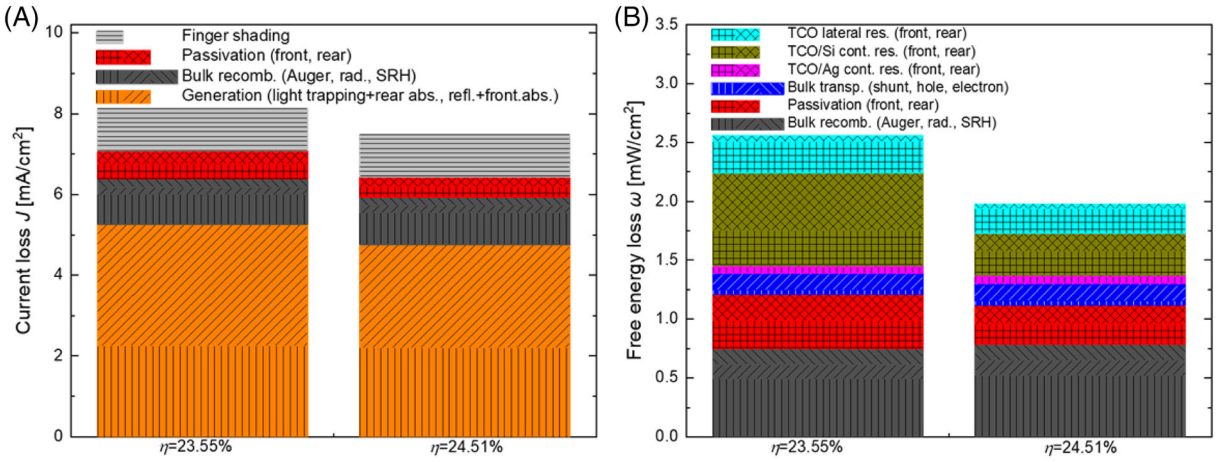


**FIGURE 7** (A) Current and (B) free energy loss analysis for old and newly certified SHJ solar cells based on Quokka3 simulation

efficiency quickly. This can be realized by using multiple TCO layers to simultaneously meet both optical and electrical requirements.

## 4 | CONCLUSIONS

In this paper, we demonstrated a route towards high-efficiency SHJ solar cells. By using a denser and thinner second part of the intrinsic a-Si:H layer, a reduced vertical rear resistance loss was achieved. This favored vertical carrier transport and led to a higher *FF*. It was also shown that by inserting a thin $MgF_2$ before Ag back reflector preparation, one could obtain a higher $J_{sc}$ gain due to the reduced plasmonic absorption. Finally, we were able to improve the efficiency from certified 23.55% to 24.51% on a total M2 area, mainly driven by *FF* and $J_{sc}$ improvement. A detailed loss analysis based on the Quokka3 simulation confirmed the design principles and also gave us some insights on how to further improve the cell efficiency, such as using more transparent wide bandgap window layers or applying multiple TCO layers which considers both optical and electrical performance.

### ACKNOWLEDGEMENTS

The authors gratefully acknowledge the funding of the German Federal Ministry of Economic Affairs and Energy in the framework of the STREET project (grant: 0324275E), TUKAN project (grant: 0324198D), and TOUCH project (grant: 0324351). The authors also want to thank the HEMF (Helmholtz Energy Materials Foundry) infrastructure funded by the (HGF) Helmholtz association and LONGi company for wafer supply.

### DATA AVAILABILITY STATEMENT

Research data are not shared.

### ORCID

*Weiyuan Duan* https://orcid.org/0000-0002-0904-3360
*Andreas Lambertz* https://orcid.org/0000-0001-8275-6837
*Karsten Bittkau* https://orcid.org/0000-0001-5381-2967
*Depeng Qiu* https://orcid.org/0000-0001-5558-7767
*Kaifu Qiu* https://orcid.org/0000-0002-2376-6928
*Uwe Rau* https://orcid.org/0000-0003-3526-3081
*Kaining Ding* https://orcid.org/0000-0002-2029-6254

### REFERENCES

1. Liu Y, Li Y, Wu Y, et al. High-Efficiency Silicon Heterojunction Solar Cells: Materials, Devices and Applications. *Mater Sci Eng*. 2020;142:100579. https://doi.org/10.1016/j.mser.2020.100579
2. Wolf SD, Descoeudres A, Holman ZC, Ballif C. High-efficiency silicon heterojunction solar cells: a review. *Greenpeace*. 2012;2(1):7-24. https://doi.org/10.1515/green-2011-0018
3. Taguchi M, Yano A, Tohoda S, et al. 24.7% record efficiency HIT solar cell on thin silicon wafer. *IEEE J Photovoltaics*. 2014;4(1):96-99. https://doi.org/10.1109/JPHOTOV.2013.2282737
4. Adachi D, Hernandez JL, Yamamoto K. Impact of carrier recombination on fill factor for large area heterojunction crystalline silicon solar cell with 25.1% efficiency. *Appl Phys Lett*. 2015;107(23):233506. https://doi.org/10.1063/1.4937224
5. Hanergy sets new efficiency record for heterojunction cell. https://www.pv-magazine.com/2019/08/08/hanergy-sets-new-efficiency-record-for-heterojunction-module/
6. Ru X, Qu M, Wang J, et al. 25.11% efficiency silicon heterojunction solar cell with low deposition rate intrinsic amorphous silicon buffer layers. *Solar Energy Mater Sol Cells*. 2020;215:110643. https://doi.org/10.1016/j.solmat.2020.110643
7. GS-Solar's mass produced HJT cell achieves conversion efficiency of 25.2%. http://www.pvtime.org/gs-solars-mass-produced-hjt-cell-achieves-conversion-efficiency-of-25-2/
8. Australian startup sets 25.54% efficiency record for silicon cell. https://www.pv-magazine.com/2021/09/10/australian-startup-sets-25-54-efficiency-record-for-silicon-cell/
9. Holman Z, Decoeudres A, Barraud L, et al. Current loss at the front of silicon heterojunction solar cells. *IEEE J Photovolt*. 2012;2(1):7-15. https://doi.org/10.1109/JPHOTOV.2011.2174967
10. Green M, Dunlop E, Ebinger J, Yoshita M, Kopidakis N, Ho-Baillie A. Solar cell efficiency tales (Version 55). *Prog Photovolt Res Appl*. 2020;28(1):3-15.
11. Qiu D, Duan W, Lambertz A, et al. Front contact optimization for rear-emitter SHJ solar cells with ultra-thin n-type nanocrystalline silicon oxide. *Solar Energy Mater Sol Cells*. 2020;209:110471. https://doi.org/10.1016/j.solmat.2020.110471

12. Mazzarella L, Morales-Vilches A, Korte L, Schlatmann R, Stannowski B. Ultrathin nanocrystalline n-type silicon oxide front contact layers for rear-emitter silicon heterojunction solar cells. *Sol Energy Mater Sol Cells*. 2018;179:386-391. https://doi.org/10.1016/j.solmat.2018.01.034
13. Smirnov V, Lambertz A, Moll S, et al. Doped microcrystalline silicon oxide alloys for silicon-based photovoltaics: optoelectronic properties, chemical composition, and structure studied by advanced characterization techniques. *Phys Status Solidi*. 2016;213(7):1814-1820. https://doi.org/10.1002/pssa.201533022
14. Mazzarella L, Kirner S, Gabriel O, et al. Nanocrystalline silicon emitter optimization for Si-HJ solar cells: substrate selectivity and $CO_2$ plasma treatment effect. *Phys Status Solidi A*. 2016;214(2):1532958. https://doi.org/10.1002/pssa.201532958
15. Fioretti A, Boccard M, Monnard R, Ballif C. Low-temperature p-type microcrystalline silicon as carrier selective contact for silicon heterojunction solar cells. *IEEE J Photovolt*. 2019;9(5):1158-1165. https://doi.org/10.1109/JPHOTOV.2019.2917550
16. Umishio H, Sai H, Koida T, Matsui T. Nanocrystalline-silicon hole contact layers enabling efficiency improvement of silicon heterojunction solar cells: impact of nanostructure evolution on solar cell performance. *Prog Photovolt*. 2021;29(3):344-356. https://doi.org/10.1002/pip.3368
17. Richter A, Hermle M, Glanz S. Reassessment of the limiting efficiency for crystalline silicon solar cells. *IEEE J Photovol*. 2013;3(4):1184-1191. https://doi.org/10.1109/JPHOTOV.2013.2270351
18. Kökbudak G, Müller R, Feldmann F, Fell A, Turan R & Glunz S. On the determination of the contact resistivity for passivating contacts using 3D simulations, 33rd EU PVSEC, Amsterdam, 2017. https://doi.org/10.4229/EUPVSEC20172017-2AO.4.3
19. Fell A. A free and fast three-dimensional/two-dimensional solar cell simulator featuring conductive boundary and quasi-neutrality approximations. *IEEE Trans Electron Devices*. 2013;60(2):733-738. https://doi.org/10.1109/TED.2012.2231415
20. Fell A, Schön J, Schubert M, Glunz S. The concept of skins for silicon solar cell modeling. *Sol Energy Mater sol Cells*. 2017;173:128-133. https://doi.org/10.1016/j.solmat.2017.05.012
21. Kim S, Dao V, Shin C, et al. Low defect interface study of intrinsic layer for c-Si surface passivation in a-Si:H/c-Si heterojunction solar cells. *Thin Solid Films*. 2012;521:45-49. https://doi.org/10.1016/j.tsf.2012.03.074
22. Zhao L, Diao H, Zeng X, Zhou C, Li H, Wang W. Comparative study of the surface passivation on crystalline silicon by silicon thin films with different structures. *Physica B*. 2010;405(1):61-64. https://doi.org/10.1016/j.physb.2009.08.024
23. Fujiwara H, Kondo M. Impact of epitaxial growth at the heterointerface of a-Si:H/c-Si solar cells. *Appl Phys Lett*. 2007;90:013503. https://doi.org/10.1063/1.2426900
24. Liu W, Zhang L, Chen R, et al. Underdense a-Si:H film capped by a dense film as the passivation layer of a silicon heterojunction solar cell. *J Appl Phys*. 2016;120(17):175301. https://doi.org/10.1063/1.4966941
25. Beyer W, Abo Ghazala MS. Absorption strengths of Si-H vibrational modes in hydrogenated silicon. *Mater Res Soc Symp Proc*. 1998;507:601. https://doi.org/10.1557/PROC-507-601
26. Langford A, Fleet M, Nelson B, Lanford W, Maley N. Infrared absorption strength and hydrogen content of hydrogenated amorphous silicon. *Phys Rev B*. 1992;45(23):13367-13377. https://doi.org/10.1103/PhysRevB.45.13367
27. Shimizu S, Kondo M, Matsuda A. A highly stabilized hydrogenated amorphous silicon film having very low hydrogen concentration and an improved Si bond network. *J Appl Phys*. 2005;97:033522. https://doi.org/10.1063/1.1846132
28. Kageyama S, Akagawa M, Fujiwara H. Dielectric function of a-Si:H based on local network structures. *Phys Rev B*. 2011;83(19):195205. https://doi.org/10.1103/PhysRevB.83.195205
29. Müllerova J, Sutta P, van Elzakker G, Zeman M, Mikula M. Microstructure of hydrogenated silicon thin films prepared from silane diluted with hydrogen. *Appl Surf Sci*. 2008;254(12):3690-3695. https://doi.org/10.1016/j.apsusc.2007.10.069
30. Descoeudres A, Barraud L, De Wolf S, et al. Improved amorphous/crystalline silicon interface passivation by hydrogen plasma treatment. *Appl Phys Lett*. 2011;99:123506. https://doi.org/10.1063/1.3641899
31. Hadjadj A, Larbi F, Gilliot M, Cabarrocas P. Etching of a-Si:H thin films by hydrogen plasma: a view from in situ spectroscopic ellipsometry. *J Chem Phys*. 2014;141:084708. https://doi.org/10.1063/1.4893558
32. Holman Z, Filipic M. Infrared light management in high-efficiency silicon heterojunction and rear-passivated solar cells. *J Appl Phys*. 2013;113(1):013107. https://doi.org/10.1063/1.4772975
33. Cruz A, Wang E, Morales-Vilches A, et al. Effect of front TCO on the performance of rear-junction silicon heterojunction solar cells: insights from simulations and experiments. *Solar Energy Mater Sol Cells*. 2019;195:339-345. https://doi.org/10.1016/j.solmat.2019.01.047
34. Holman Z, De Wolf S, Ballif C. Improving metal reflectors by suppressing surface plasmon polaritons: a priori calculation of the internal reflectance of a solar cell. *Light: Sci Appl*. 2013;2(10):e106. https://doi.org/10.1038/lsa.2013.62
35. Haug FJ, Söderström T, Cubero O, Terrazzoni-Daudrix V, Ballif C. Plasmonic absorption in textured silver back reflectors of thin film solar cells. *J Appl Phys*. 2008;104(6):0645509. https://doi.org/10.1063/1.2981194
36. Kray D, Hermle M, Glunz S. Theory and experiments on the back side reflectance of silicon wafer solar cells. *Prog Photovoltaics: Res Appl*. 2008;16(1):1-15. https://doi.org/10.1002/pip.769
37. Woehrle N, Greulich J, Schwab C, Glatthaar M, Rein S. A predictive optical simulation model for the rear-surface roughness of passivated solar cells. *IEEE J Photovoltaics*. 2013;3(1):175-182. https://doi.org/10.1109/JPHOTOV.2012.2215013
38. Davis K, Kaiyun J, Demberger C, et al. Investigation of the internal back reflectance of rear-side dielectric stacks for c-Si solar cells. *IEEE J Photovoltaics*. 2013;3(2):641-648. https://doi.org/10.1109/JPHOTOV.2012.2233861
39. Holman Z, Filipic M, Lipovsek B, et al. Parasitic absorption in the rear reflector of a silicon solar cell: Simulation and measurement of the sub-bandgap reflectance for common dielectric/metal reflectors. *Solar Energy Mater Sol Cells*. 2014;120:426-430. https://doi.org/10.1016/j.solmat.2013.06.024
40. Campbell P, Wenham S, Green M. Light trapping and reflection control in solar cells using titled crystallographic surface textures. *Solar Energy Mater Sol Cells*. 1993;31(2):133-153. https://doi.org/10.1016/0927-0248(93)90046-6
41. Duan W, Bittkau K, Lambertz A, et al. Improved infrared light management with transparent conductive oxide/amorphous silicon back reflector in high-efficiency silicon heterojunction solar cells. *Sol RRL*. 2021;5(3):2000576. https://doi.org/10.1002/solr.202000576
42. Cattin J, Petri D, Geissbühler J, Despeisse M, Ballif C, Boccard M. Transferability of the light-soaking benefits on silicon heterojunction cells to modules. *Appl Phys*. 2021. Preprint


**How to cite this article:** Duan W, Lambertz A, Bittkau K, et al. A route towards high-efficiency silicon heterojunction solar cells. *Prog Photovolt Res Appl*. 2022;30(4):384-392. doi:10.1002/pip.3493